JTTEE5
DOI: 10.1007/s11666-015-0240-4
1059-9630/$19.00 © ASM International

Influence of Cold-Sprayed, Warm-Sprayed, and Plasma-Sprayed Layers Deposition on Fatigue Properties of Steel Specimens

J. Cizek, M. Matejkova, I. Dlouhy, F. Siska, C.M. Kay, J. Karthikeyan, S. Kuroda, O. Kovarik, J. Siegl, K. Loke, and Khiam Aik Khor

(Submitted August 12, 2014; in revised form February 20, 2015)

Titanium powder was deposited onto steel specimens using four thermal spray technologies: plasma spray, low-pressure cold spray, portable cold spray, and warm spray. The specimens were then subjected to strain-controlled cyclic bending test in a dedicated in-house built device. The crack propagation was monitored by observing the changes in the resonance frequency of the samples. For each series, the number of cycles corresponding to a pre-defined specimen cross-section damage was used as a performance indicator. It was found that the grit-blasting procedure did not alter the fatigue properties of the steel specimens (1% increase as compared to as-received set), while the deposition of coatings via all four thermal spray technologies significantly increased the measured fatigue lives. The three high-velocity technologies led to an increase of relative lives to 234% (low-pressure cold spray), 210% (portable cold spray), and 355% (warm spray) and the deposition using plasma spray led to an increase of relative lives to 303%. The observed increase of high-velocity technologies (cold and warm spray) could be attributed to a combination of homogeneous fatigue-resistant coatings and induction of peening stresses into the substrates via the impingement of the high-kinetic energy particles. Given the intrinsic character of the plasma jet (low-velocity impact of semi/molten particles) and the mostly ceramic character of the coating (oxides, nitrides), a hypothesis based on non-linear coatings behavior is provided in the paper.

Keywords cold spray, fatigue, grit-blast, plasma spray, residual stresses, titanium, warm spray

1. Introduction

Thermal spray is a family of processes used for deposition of protective coatings onto substrates (Ref 1). The fabricated coatings are relatively thick (up to hundreds μm) and generally exhibit a heterogeneous structure, as a consequence of the unique character of the respective technologies deposition.

Of the processes, plasma spraying (PS) ranks among the most universal methods in terms of material selection (Ref 2). In the process, materials in the form of powder are injected into a hot jet of ionized gases. Within the short dwelling time, the powder particles are accelerated (Ref 3), partially or fully molten, and impinged onto a prepared substrate. At the impact, they solidify, creating the so-called splats, fundamental elements of the produced coatings. The high temperatures of the plasma spray process are generally also regarded a major disadvantage, inducing several detrimental effects (e.g., oxidation, phase transformations, internal stresses).

Cold spray (CS) is a novel technology resolving the temperature issues of the preceding technologies: the powder particles are deposited in a solid state and the kinetic energy of impact (plastic deformation of supersonic particles) is used for the coating formation instead (Ref 4). In-flight oxidation of the sprayed material, a process intensified at elevated temperatures, is suppressed, and the absence of oxides improves the intrinsic bonding strength, resulting in one of the highest adhesion strengths among thermal spray processes (Ref 4). Due to the lower porosity content and increased value of elastic moduli, the cold-sprayed coatings are more susceptible to deformation-induced cracking (Ref 5). As primary and secondary thermal stresses are negligible in cold spray, peening stresses originating from the deformation upon particle impingement become dominant. Complex computational studies (e.g., Assadi et al. (Ref 6), Schmidt et al. (Ref 7), Suhonen et al. (Ref 8)) were carried out in order to understand the stress build up during cold spray. The requirement for the plasticity of the materials currently presents the major handicap of

J. Cizek, M. Matejkova and **I. Dlouhy**, Netme Centre, Institute of Materials Science and Engineering, Brno University of Technology, Brno, Czech Republic; **F. Siska**, Institute of Physics of Materials, Czech Academy of Sciences, Brno, Czech Republic; **C.M. Kay** and **J. Karthikeyan**, ASB Industries, Inc., Barberton, OH; **S. Kuroda**, National Institute for Materials Science, Tsukuba, Japan; **O. Kovarik** and **J. Siegl**, Czech Technical University, Prague, Czech Republic; **K. Loke**, Singapore Technologies-Kinetics, Tuas, Singapore; and **Khiam Aik Khor**, School of Mechanical and Aerospace Engineering, Nanyang Technological University, Singapore, Singapore. Contact e-mail: cizek@fme.vutbr.cz.

Published online: 17 April 2015

the process as e.g. pure ceramic materials could not be deposited.

Warm spray (WS) represents the newest addition into the thermal spray family. Developed as a modification of HVOF (high velocity oxy-fuel) process, the particles are deposited in a solid state due to additional cooling by inert gas (usually nitrogen) flow in the gun mixing chamber attached to the gun barrel (Ref 9). In terms of in situ temperatures of the particles, warm spray ranks between cold spray and HVOF spray technologies.

Considering the respective build-up mechanisms, the deposition of the coatings via different technologies may induce a range of diverse effects on the substrate's characteristics. Among the most important changes are the development of internal stresses (Ref 10), influencing load-resistance parameters and triggering different failure mechanisms under external loading. A typical example is a change in measured fatigue endurance of coated components under cyclic loading (Ref 11-13). It was demonstrated that the high-temperature deposition of the layers plays a crucial role in the fatigue properties of the specimens. For cold spray technology, studies investigating the influence of different coating materials on the fatigue properties of bodies have been published (e.g. Refs 14-16).

The aim of this work was to define the influence of various thermal spray technologies on the fatigue properties of coated specimens and to identify the factors contributing to the component failure. Such task differs significantly from the fatigue characterization of bulk materials. Typically, the surface properties of the bulks are ''standardized'' prior to the tests, for example, by surface polishing. However, no such procedure could be implemented for the coatings as the respective surface properties play a crucial role in the fatigue properties of the coated components. Therefore, the focal point of the performed tests was the performance of the steel substrates, to which the whole test setup and loading were adjusted. Consequently, the deposited coatings were considered as an external factor in the entire study and the fatigue test characterized only the particular combination of substrate-coating with its inherent surface properties such as material composition and microstructure, residual stress field, adhesive and cohesive strengths, geometry (coating thickness), porosity, etc. Four thermal spray processes were involved for mutual comparison: atmospheric plasma spray, portable cold spray, low-pressure cold spray, and warm spray. Their respective performances were compared to as-received set and grit-blasted set and the causes of the failure were investigated for each set.

2. Experimental Setup

2.1 Materials

Due to a wide range of technologies used in the study, the selection of the coating material was influenced by two factors: its physical-mechanical properties, and its suitability for all the processes from the point of view of particle sizes. A commercially available Ti powder acceptable for biomedical applications (Amperit 155.054, HC Starck, Germany, 10-45 μm) was selected and used throughout the study. The selection further facilitated comparison with the previous study carried out using Ti powder on TiAl4V substrates (Ref 11).

In order to ensure identical conditions for all deposition technologies, the as-received powder was not sieved. Its particle size distribution was specified by laser analysis measured using Fritsch Nanoanalysette 22 device. The powder sizes were determined as 13.6-90.3 μm (5-95% quantile). The mean particle size was ~43.6 μm and no <5 μm dust was detected. With respect to the requirements of the four used technologies, the particle sizes are optimal for plasma and warm spray systems. However, cold spray technology generally works with smaller particle sizes, ideally <45 μm (Ref 4). The somewhat bigger Ti particles may have affected the porosity content in the coatings, as will be discussed in section 3.1.

The powder exhibited angular morphology, as could be seen from Fig. 1(a), which corresponded to the fused and crushed production route. According to in-flight measurement studies in cold spray (e.g., Helfritsch and Trexler (Ref 17) or Fukanuma et al. (Ref 18)), the angular morphology is beneficial for attaining higher in-flight velocities during cold spray deposition, effectively counteracting the negative effect of the bigger particle sizes. As an inherent consequence of the fused and crushed production route, formation of small pores in the powder particles is frequently observed. The analysis of the particle cross section determined the internal porosity levels of the Ti powder as 0.5% (Fig. 1b).

The chemical composition of the powder provided by the manufacturer indicated no impurities with maximum oxygen content of 0.3 at.%. The powder was determined as 100% α-Ti by XRD analysis.

As a substrate material, 1.0038 grade cold-rolled steel was used (S235JRC, 0.19 wt.% carbon, R_m = 340-470 MPa). The material was selected due to its ease of machining and connection to the previous studies (Ref 19). The cold rolling induced compressive stresses into the material (Ref 20). However, as all substrates used in the study were fabricated via this route, the cold rolling did not affect the measured relative ratio of fatigue performances of the respective sets.

2.2 Sample Preparation and Characterization

Due to the specific nature of the subsequent cyclic loading experiment, specimen substrates were fabricated from 4-mm-thick steel sheets in a geometry corresponding to Fig. 2. The specimens were designed in order to localize the area of prospective crack initiation sites and facilitate more accurate crack detection. The symmetric design of the specimens allowed carrying out two measurements per sample, further increasing the obtained data reliability. Chemical degreasing was carried out in order to remove any oil or contaminant films from the substrate surfaces.

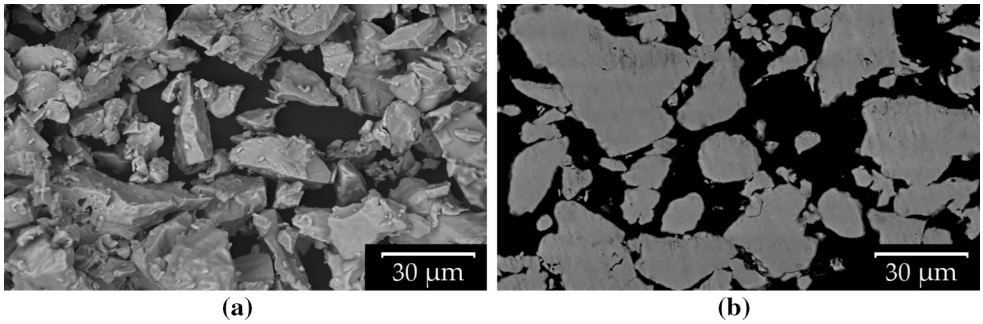

Fig. 1 (a) Morphology and (b) cross section of used Ti powder

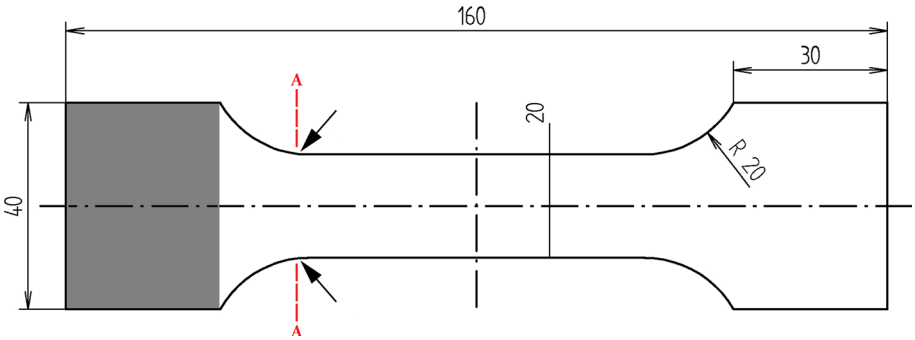

Fig. 2 Geometry of the fatigue test specimens. Arrows indicate crack initiation sites, gray area represents cantilever clamping area, A-A section shows the orientation of sample fracture surfaces

Six sets of samples were prepared. As a benchmark for relative performance indication, non-modified substrates with no coating or grit blasting were used (as-received, AR). Usually, grit-blasting procedure is employed prior to the coating process to improve coatings-substrate adhesion and the interface quality (Ref 21, 22). As the grit-blasting procedure may induce (compressive) stresses into the near-surface areas (Ref 11), it was necessary to test its influence. For that purpose, a blend of SiC and Al_2O_3 particles (380-760 µm) was used to produce second, grit-blasted set (GB). The average surface roughness of the set reached R_a = 3.15 µm and no further coating was applied.

Four coated sets were then produced using various thermal spray technologies. The Ti powder was deposited onto both major faces of the substrates (Fig. 2) with the target thickness of 500 µm. The thickness was selected to accentuate the effect of the layer addition on the properties of the coated samples while restraining a spontaneous delamination, spallation, and cracking resulting from the residual stresses build up (Ref 1).

Atmospheric plasma spray system (Praxair 4600 Module equipped with SG-100 plasma gun) with Ar/He main/auxiliary gases was employed for fabrication of PS set. Cold spray assembly used to produce the CS-L set (low-pressure cold spray, ITAM, Russian Academy of Science) was equipped with wear-resistant ceramic Laval nozzle and used purified He as the working and feeder gas. The helium gas temperature was maintained at 770 K, well below the temperature of α-Ti → β-Ti transition (1155 K) and the temperature indicated for initiation of the reaction with oxygen to form TiO_2 (1470 K) (Ref 23). Portable ASB 2000-2 cold spray system was then used (CS-P) with nitrogen as the main propellant gas at 620 K. Lastly, warm spray was used for coatings deposition (WS) with kerosene used as a fuel. The respective spray parameters pertaining to the individual technologies are shown in Table 1.

The microstructure and thickness of the fabricated coatings was evaluated on polished samples using light microscopy (Axio Observer Z1m, Zeiss) and FEG-SEM (Ultra Plus, Zeiss). In order to obtain information on the coatings porosity, image analysis was carried out (ImageJ software, contrast thresholding). At least 10 images were evaluated at two different SEM magnifications (×100, ×500). The surface roughness indicators (R_a, R_z) of the individual sets were measured according to ISO: 4287 standard (Ref 24) in two perpendicular directions to affect the potential effect of the spray direction. For the measurements, TR200 portable profilometer was used (TimeGroup, Inc., China) with the measurement length of 0.8 × 5 mm and range of ±80 µm.

To obtain information on the coating hardness, 10 indentations were carried out per sample using Vickers indentation at 200 gf load (LM247AT, Leco Corp., USA) on the polished cross sections of the deposits. Careful metallographic preparation of the samples was employed in order to minimize the microstructural effect observed by Chicot et al. (Ref 25). The indentation load was selected with regard to the heterogeneous structure of the coatings (mainly PS) with the aim of providing the average microhardness value of the sprayed material. The typical

Table 1 Spray parameters for PS, CS-L, CS-P, and WS coatings deposition

Plasma spray		Cold spray	CS-L	CS-P	Warm spray	
Net power	15 kW	Gas used	helium	nitrogen	Flow of nitrogen	1000 l · min^{-1}
Flow of main gas (Ar)	47.2 l · min^{-1}	Gas pressure	1.3 MPa	2.0 MPa	Flow of oxygen	714 l · min^{-1}
Flow of auxiliary gas (He)	37.8 l · min^{-1}	Gas temperature	770 K	620 K	Flow of kerosene	347 ml · min^{-1}
Flow of carrier gas (Ar)	7.11 · min^{-1}				Barrel length	200 mm
Feedrate frequency	4 rpm	Feedrate frequency	70 Hz	200 rpm	Powder feedrate	30 g · min^{-1}
Spray distance	120 mm	Spray distance	12 mm	25 mm	Spray distance	200 mm

diagonal length of the indentation under such load reached 40-60 μm, spanning a number of individual flattened splats in the coating structure.

To assess the influence of the used surface technologies on the change in properties of the uppermost layers of the substrate material, series of indentation tests were performed using NHT^2 nano-indenter device (CSM Instruments, Switzerland; Berkovich indenter, 30 mN maximum load, 15 s dwell time). The hardness profiles of the material were measured perpendicularly to the substrate-coating interface with 10 μm spacing toward the center of the substrate (200 μm profile depth).

The phase composition of the deposited layers was determined using XPert Pro X-ray diffractometer (Co K_α, K_β absorption filter) equipped with XCelerator detector (PANalytical B.V.). Rietveld analysis of the acquired XRD spectra (Ref 26) was carried out in order to quantify the chemical composition and address the respective changes pertaining to composition of the initial powder feedstock. Merging two measured patterns prior to the analysis aided in removing casual errors in the detection (e.g., accidental noise delta function peaks). The standardized patterns for the particular phases were collected from ICSD databases. The analysis was complemented by EDX (EDAX XL-30) analyses for elemental composition.

2.3 Fatigue Experiments

The fatigue tests were carried out on an electromagnetic computer controlled resonance fatigue test device developed at Czech Technical University (Fig. 3) (Ref 27). The flat specimens were loaded by symmetrical cyclical bending (as cantilever beams, $\sigma_m = 0$, $R = -1$) with a fixed free end deflection amplitude $U = \pm$ 4 mm. The tests were performed at room temperature and the critical area of the samples was air cooled.

For high cycle fatigue, the loading amplitude needs to be chosen so that only limited amount of plastic strain develops at the specimen surface. On the other hand, reasonably short fatigue lives are desirable for time constraints of the testing process. Combining the two requirements, ~ 200,000 cycles target fatigue lives of the uncoated specimens were selected for our study. To select the corresponding nominal loading strain amplitude, the median method presented in (Ref 28) can be used. The required input for the calculation, tensile strength of the material, was estimated using an additional tensile test as $R_m = 480$ MPa. For these conditions, a strain amplitude of 1.33×10^{-3} was calculated, of which 1.10×10^{-3} pertains to elastic and 0.23×10^{-3} plastic strain at the substrate surface. The calculation therefore predicted that the test at such loading amplitude will be performed preferably in the elastic strain dominated (i.e., high cycle fatigue) mode. The corresponding sample free end deflection amplitude can be further calculated from

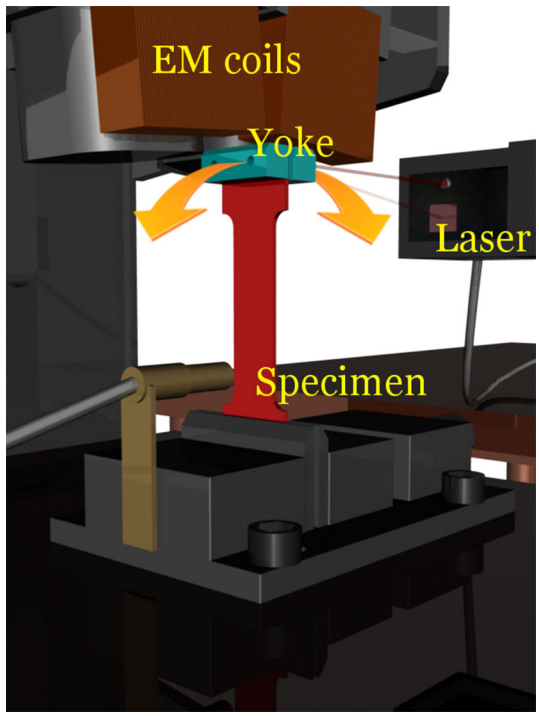

Fig. 3 The specimen loading in the developed fatigue device

$$U = \frac{\epsilon}{HC}, \qquad \text{(Eq 1)}$$

where U is the free end deflection amplitude in mm, ϵ is the longitudinal strain at the crack initiation site on the substrate surface (indicated by arrows in Fig. 2), H is the substrate thickness, and C is a calibration constant. The value of the constant was calibrated as $C = 0.08437\times 10^3$ mm^{-2} by testing auxiliary samples at different amplitudes and measuring the actual strain using a doublet of strain gages. Subsequently, the value was verified by an additional FEM simulation. For the obtained strain amplitude of 1.33×10^{-3}, a free end deflection of 3.94 mm was calculated, i.e., the deflection of 4 mm used in our study was well justified for the testing. The actual strain value under 4 mm deflection was measured as 1.35×10^{-3}.

The excitation frequency $f(N)$ corresponded to the first natural resonance frequency of the mounted specimen and

was maintained using a phase-locked loop technique. It ranged from 75 to 95 Hz, depending on the coating stiffness, thickness, and density and changed with the number of cycles N. The crack growth in the specimens induced a decrease of the natural resonance frequency. The excitation frequency decrease $df = f(\frac{N}{2}) - f(N)$ was used as a quantity reflecting the crack growth (Ref 27). As a stopping condition of the experiment, a drop of df = 3 Hz was used, corresponding to approximately 30% damage of the specimen cross section. The fatigue life of the specimen was defined as the number of cycles at the stopping condition. The obtained fatigue lives of the specimens are not affected by the variances in the damaged area due to the relatively high crack growth rate during the final stages of the experiments.

2.4 Fractographic Analysis

Liquid nitrogen was used to cool the fatigued samples below the transition temperature and the specimens were then ruptured by impact. Fractographic analysis of the fractured surfaces was then carried out using Jeol JSM-840A SEM in secondary electron mode to reflect the micromorphology of the specimen surfaces. The analysis was performed for the substrates as well as the coatings and aimed at determining the crack initiation sites and primary propagation directions.

3. Results and Discussion

3.1 Sample Characterization

The morphology of the four types of coatings is shown in Fig. 4. The structures correspond to the typical coatings produced via the four technologies: the WS and both CS technologies led to compact structure coatings due to the high in-flight velocity (kinetic energy) of the process (Ref 4, 9), while the plasma-sprayed deposits were characterized by the lamellae splats with limited amount of splashing due to the molten state impacts (Ref 29).

The coatings produced via WS technology exhibited compact morphology of the material. Within the coatings structure, individual particles could be observed due to the presence of a small oxide layer surrounding each particle. The oxide shells might have originated due to elevated temperatures of the process. The low-pressure cold spray technology produced coatings with slightly increased porosity as compared to WS set (2.3%, Table 2), with indications of individual splats in the structure. The porosity could be a consequence of the slightly bigger particle sizes of the used powder feedstock. The presence of the oxide shells was not observed. The densest coatings were obtained for the CS-P set with no distinguishable splats (porosity 0.2%). The plasma-sprayed coatings exhibited a heterogeneous, non-compact structure with relatively high porosity. Individual splats could easily be observed in the material, as well as the elongated interconnected pores along the splat contact zones.

The substrate-coatings interface was well adherent for all four coating types with no visible gap (as observed in SEM). The surface roughness of the plasma-sprayed coating was slightly lower than that of the three high-velocity technologies (Table 2). This is probably caused by enhanced conformation of the incoming (semi)molten particles to underlying surface asperities and the relatively smooth splat surfaces driven by the surface tension of the molten material prior to solidification (Ref 29).

The production using various technologies led to significant thickness variation among the respective sets (Table 2). During the fatigue test, the strain amplitude imposed at the deposit surface is given by the specimen thickness. Under the assumption of linear elastic deformation, the strain is calculated as follows:

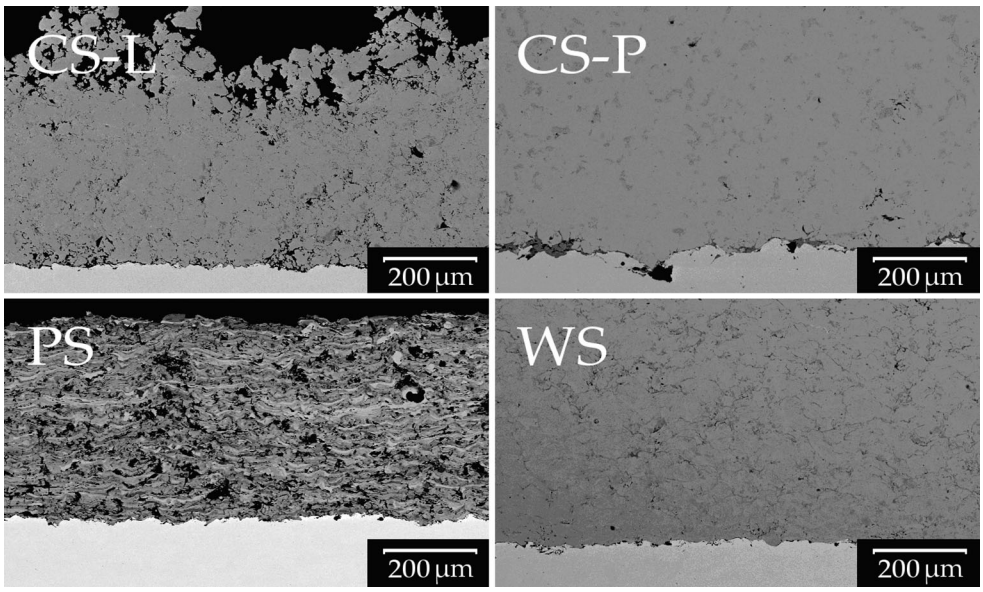

Fig. 4 The structure of the Ti coatings produced via four technologies (BSE imaging)

Table 2 Properties of the deposited coatings and results of fatigue testing of the respective six sets

Set	Coating thickness, μm	Surface roughness R_a, μm	Coating porosity, %	Coating hardness [HV0.2]	Average # of cycles [1]	Relative life R_f [1]	Resonance frequency, Hz
AR	—	0.33	—	—	222,462	1.00	79.3
GB	—	3.15	—	—	223,770	1.01	81.0
CS-L	570	5.75	2.3	69	519,696	2.34	85.1
CS-P	790	6.48	0.2	68	467,643	2.10	83.1
PS	420	4.63	11.4	562	674,176	3.03	86.5
WS	640	6.05	0.5	165	789,360	3.55	93.9

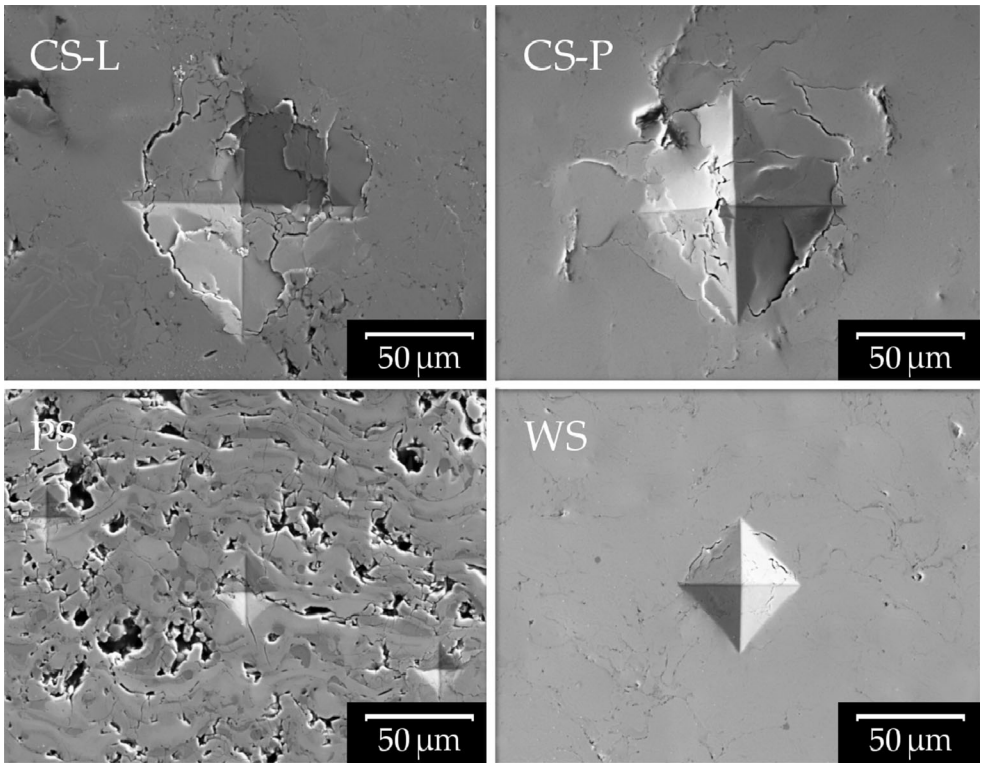

Fig. 5 Coating deformation after HV0.2 indentations

$$\epsilon = c_1 \times (\frac{H_s}{2} + h_c), \qquad \text{(Eq 2)}$$

where c_1 is a constant, H_s is the substrate thickness (4 mm), and h_c is the coating thickness. Given the numerical values of the deposited thicknesses and the strain levels in the fatigue experiment (1.3×10^{-3}, section 2.3), the maximum relative difference of the surface strain will be ~ 15% (between the PS and CS-P sets). It was shown previously (Ref 30) that the increase of Al_2O_3 coating thickness from 0.35 to 0.90 mm (~ 23% strain increase) led to 20% decrease of fatigue life. Similar results were obtained (Ref 27) for olivine $(MgFe)_2SiO_4$ (15% fatigue life decrease for a change from 0.71 to 1.31 mm coating thickness, i.e., 22% strain increase). The changes in the measured fatigue performance caused by the variations in the coating thickness were therefore one order of magnitude smaller than the observed influence of the deposition technology (Table 2). As such, it could be concluded that the variations in the coating thicknesses of the individual sets do not critically influence the measured fatigue lives and the results of the respective sets can be directly compared.

Due to the high velocity combined with solid-state impact of the CS and WS particles, extensive plastic deformation leading to intensive strain hardening of the coating material was expected (Ref 6). To assess this, microhardness of the coatings was measured. From the results (Table 2), it could be seen that both cold spray technologies produced coatings of similar hardness (~ 70 HV0.2). Given the differences in the deposition parameters (770 K helium at 1.3 MPa versus 620 K nitrogen at 2.0 MPa), it could be assumed that such values correspond to the limit hardness of Ti material after the strain hardening effect, particularly at the particle surfaces (the brittle particle interfaces may then lead to a typical fracture morphology of the deposit, section 3.3). It should be noted that the discussed limit hardness depends on the particle sizes of the powder feedstock.

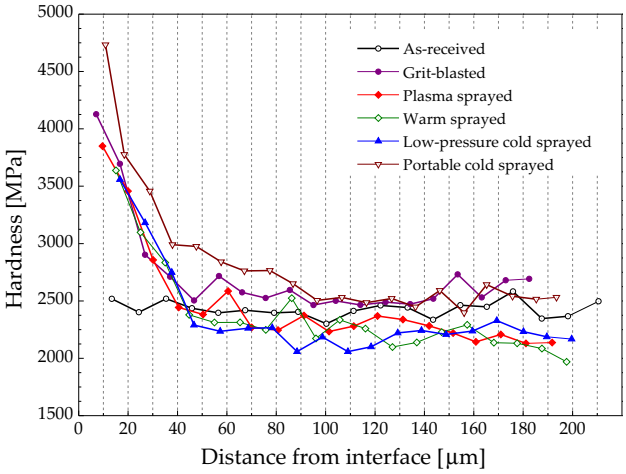

Fig. 6 Measured hardness profiles of the substrates from the six respective sets

The particle surface brittleness could cause the fragmentation of the material below the indenter observed during microhardness measurement (Fig. 5). Such behavior resulted in a decreased microhardness of the CS deposits in comparison to the WS set (165 HV0.2) and is related to the hardness loss parameter suggested by Goldbaum and coworkers (Ref 31). It appears that the higher particle temperature of the WS deposition is an efficient way for reduction of the detrimental effects of particle surface embrittlement. Further, the increased microhardness value of WS set could be contributed by the presence of small oxide particles in the coatings. The highest value of microhardness was measured for PS samples ($\sim$ 560 HV0.2). With regard to the relatively high porosity of the coating (a factor causing decrease in hardness), the substantial increase is most likely caused by the presence of TiN and TiO oxides in the structure of the coatings (Fig. 4).

The measured substrate hardness profiles confirmed the idea of the blasting technology impact on the uppermost layers of the material. As could be seen from Fig. 6, the grit-blasting procedure led to a notable increase in the hardness up to the depths of $\sim 50\,\mu$m. This effect is a direct consequence of work hardening of the steel material and was also observed in other studies, e.g., (Ref 32, 33). An effect of similar magnitude was also observed for PS, WS, and CS-L samples, i.e., the deposition of the coating via the three technologies did not lead to a further increase in the substrate material hardness. A more pronounced effect was observed in the case of CS-P set. However, it could not be safely determined whether the effect could be attributed to the deposition of the coatings or it was caused by the grit-blasting procedure carried out in the joint laboratory.

The chemical composition analysis indicated that both cold spray technologies did not alter the element or phase composition of the deposited Ti material and both coatings were found to comprise 100% α-Ti. Despite the inherent high reactivity of titanium above 770 K (Ref 34), the work gas temperature in both atmospheric processes did not trigger any reactions with oxygen or nitrogen due to short dwell time in the heated gas. Due to the increased temperatures of the WS process, slight oxidation of Ti was recorded, giving rise to 1.9 at.% Ti_3O content (measured by XRD and observed at the surfaces of the individual splats by SEM BSE mode and EDX mapping). The formation of Ti-rich non-stoichiometric Ti_3O sub-oxide phase instead of more stable TiO_2 could be attributed to incomplete oxidation of titanium particles during the flight by low diffusion of oxygen atoms into the hexagonal α-Ti lattice (Ref 35). The Rietveld analysis of the plasma-sprayed coatings XRD spectra indicated the composition of the coatings as (at.%) 37.4% TiN and 62.6% various stoichiometric titanium oxides (5.9% TiO_2-rutile, 2.6% TiO_2-anatase, 10.9% Ti_3O, 43.2% $TiO_{0.97}$, and $Ti_{1.85}O_3$ oxides), i.e., no initial Ti phase was retained during the plasma process. The presence of various compounds was confirmed by EDX point analyses of the individual phases observed in SEM BSE mode. The full transformation of Ti into TiN (fcc) and oxide phases is in accordance with other studies (Ref 11, 36, 37) and is a result of the inherent high-temperature nature of the plasma process.

3.2 Fatigue Performance

For the used setup, the average fatigue life was $R_f = 222,462$ for the as-received set (Table 2). This is in good agreement with the fatigue life of 200,000 cycles estimated from a computation at the selected strain amplitude in the critical area of the substrate according to (Ref 28). The grit-blasting procedure did not alter the fatigue life of the specimens (+1%, Fig. 7, Table 2). This result is in agreement with the previous studies for cold-rolled substrates (Ref 27), but is in contrast to the considerable influence of the grit-blasting procedure on Ti6Al4V substrates observed in (Ref 11). This difference could be attributed to influences of two contradictory factors on the two materials: beneficial effects of compressive residual stresses and strain hardening and a detrimental micro-notch effect. The former were identified in identical material that was subjected to a blasting procedure in the recent study (Ref 19) and are indirectly supported by the measured increase in the substrate hardness after the blasting procedure. The latter is a consequence of the significant increase in surface roughness ($\sim 10\times$) upon blasting and its negative effect was shown by Price et al. (Ref 15) (rotating bend test). This result suggests that from the fatigue point of view, for high in-flight velocity technologies (WS, CS), the grit-blasting procedure of steel substrates should either not be carried out as it does not benefit the fatigue resistance and might encourage fatigue crack initiation, or the blasting medium should be of spherical, non-angular morphology (e.g., bead blasting).

The deposition of coatings via all four technologies contributed to a substantial increase in the average fatigue lives, ranging from +110% to +255% (Table 2). In general, it could be assumed that the respective increases are induced by alteration of the total (loading+residual) stress field in coatings and substrates, by the presence of fatigue-resistant coatings, or by the constraint imposed on the substrate defects by the coating.

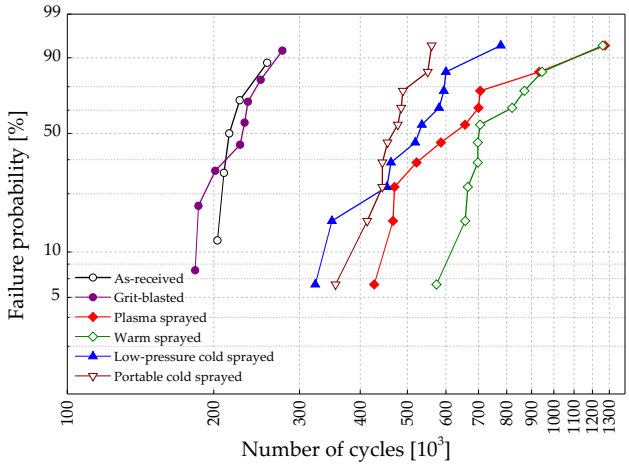

Fig. 7 Weibull (failure) probability plot of the six sample series

In the case of the PS set, redistribution of the residual stresses in substrates similar to that observed in (Ref 19) could be expected and its compressive nature may be retained. During the deposition, the metal powder feedstock was completely transformed into a coating of ceramic nature (→ nitrides, oxides). However, the formation of thermal contraction stresses (originating due to the difference in thermal expansion coefficients of the coating and the substrate (Ref 1)) is probably not the major factor triggering the recorded increase in fatigue lives, as the CTE mismatch between the steel ($CTE_{1.0038} = 11.62 \times 10^{-6}\,K^{-1}$, (Ref 38)) and the coating materials is not significant ($CTE_{TiN} = 9.35 \times 10^{-6}\,K^{-1}$, $CTE_{TiO_2-rutile} = 9.37 \times 10^{-6}\,K^{-1}$, $CTE_{TiO_2-anatase} = 8.42 \times 10^{-6}\,K^{-1}$, no literature on the $TiO_{0.97}$, $Ti_{1.85}O_3$, Ti_3O, (Ref 39)). Instead, the $\sim 3\times$ increase could be attributed to the nonlinear behavior of the coatings. As shown in section 3.1, the PS coatings consist of layers of splats with clearly pronounced porosity, intersplat decohesion, and cracks. As described by Kroupa (Ref 5), the presence of these imperfections leads to a nonlinear behavior of the deposit characterized by large difference between the tensile and the compressive stiffness. Musalek et al. (Ref 40) have shown that the difference in the two corresponding moduli could amount to $10\times$ in the case of a ceramic coating. This, in turn, induces a decrease of the effective stress amplitude in the substrate near its surface. For this type of coating, it could be expected that the fatigue damage does not occur in the form of a major fatigue crack propagation, but could be rather described by opening of a distributed network of pores and micro-cracks over a relatively large volume (Ref 19). As a consequence, initiation of a major crack in the substrate is delayed by the induced decrease of the substrate loading amplitude.

Similar increase in the fatigue lives values was observed for the two cold spray technologies ($>2\times$ longer lifetime) and the most favorable effect was observed for specimens with warm-sprayed coatings ($3.55\times$ lifetime). For the three high-kinetic energy technologies, the peening effect generated by the impacts of the solid particles is expected to introduce compressive stresses within the deposit and further increase the extent of the compressive residual stress in the uppermost layers of the substrates (Ref 4). Upon superimposing with the external load, the resulting shift of the total (loading+residual) stresses effectively decreases the stress ratio R and the effective value of stress intensity factor, leading to an increase in the fatigue life.

Further to that, the detrimental effect of micro-notches produced in grit blasting could be suppressed by the high-velocity deposition, as the first incoming layer of Ti material partially obliterated the rough surface structure. This phenomenon was observed during an additional experiment: using mechanical force, the coatings were partially delaminated from the substrates. The exposed substrate areas exhibited smoother surfaces as compared to the grit-blasted state. This was subsequently confirmed by the surface roughness measurements of the obliterated structure, leading to slightly lower $R_a = 2.49\,\mu m$ (versus $R_a = 3.15\,\mu m$ after grit blasting).

The described contribution of the two factors may lead to two different modes of crack initiation and propagation of the CS and WS sets, respectively. In both modes, it is assumed that the compressive stress of the Ti deposit, its low elastic modulus, and high yield stress of bulk Ti make it a fatigue-resistant element.

- due to its high density, the coating material could be considered ''near-bulk''. As such, the fatigue cracks initiate in the coatings surface and propagate through the deposit before being transferred to the substrate. The increase in the fatigue life is then determined by the increased fatigue resistance of the coating.
- the magnitude of the effective stress intensity factor at the coating surface is directly linked to its elastic modulus and the nature of the residual stress. The combination of lower elastic modulus of Ti (116 GPa, (Ref 11)) and the compressive residual stress field disallows crack initiation on a coating surface and, as a result, the fatigue cracks initiate in the substrate instead. The intact dense coating subsequently constrains (Ref 19) the plastic deformation of the substrate, yielding the specimen a longer fatigue life.

3.3 Fractographic Analysis

The performed fractographic analysis confirmed that the failure character corresponded to cyclic bending loading. The analysis clearly distinguished the fatigue cracks and the final static rupture of the substrate material. The fatigue crack initiation sites and crack propagation directions in the substrates were identified. However, the fracture micromorphology of the deposits did not provide enough fractographic features to clearly identify the initiation sites and crack propagation directions in the coatings.

The number of substrate crack initiation sites and their respective localization and crack propagation direction differed for the investigated sets. In all cases with the exception of the AR set, the cracks initiated at grit

blasting-induced micro-notches or at embedded blasting particles. Their respective initiation mode was inter-granular, followed by a subsequent trans-granular propagation mode via a striation mechanism. The fatigue crack propagation occurred predominantly in quarter- or half-ellipsoidal form and merging of two cracks was observed occasionally. For AR, GB, and CS sets, multiple initiation sites on the major specimen faces (mostly close to the specimen edges) were observed (Fig. 8). A typical propagation direction in such cases was perpendicular to the substrate-coating interface (an illustration of the phenomenon is provided in Fig. 9a) and was previously observed for sets with neutral influence on the fatigue life (Ref 11, 19). Similarly, the initiation sites of the cracks in PS set were observed on the major face. However, their number was reduced (often, one initiation site was observed per specimen) and they were predominantly localized in the vicinity of the specimen edges (Fig. 8). In contrast to other sets, the crack initiation sites in the WS substrates completely avoided the major faces and were located at the specimen sides instead (Fig. 9b). This mode of failure supports the hypothesis that the high fatigue resistance of the coating resulted in crack initiation in the substrates.

The PS coatings failure did not follow a pattern typical for plasma sprayed coatings. The microstructure of the deposit observed from Fig. 4 is not apparent on the fracture surface. The PS coatings contained a significant number of vertical cracks. Due to this fact and the character of the contact between adjacent splats, the cracks propagated in one plane over several splats (interconnecting of the pre-existing cracks), without regard to individual splat boundaries. Fragmentation of the PS deposit material is the only sign describing the fatigue

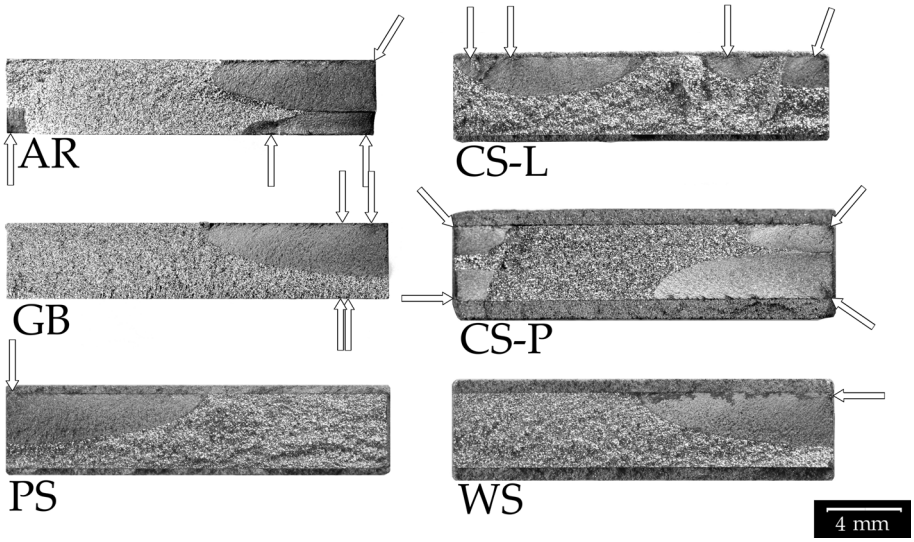

Fig. 8 Typical fractured surfaces and fatigue crack shapes of the six tested sets. The arrows indicate the cracks initiation sites and propagation directions. The orientation of the surfaces could be seen from A-A section in Fig. 2

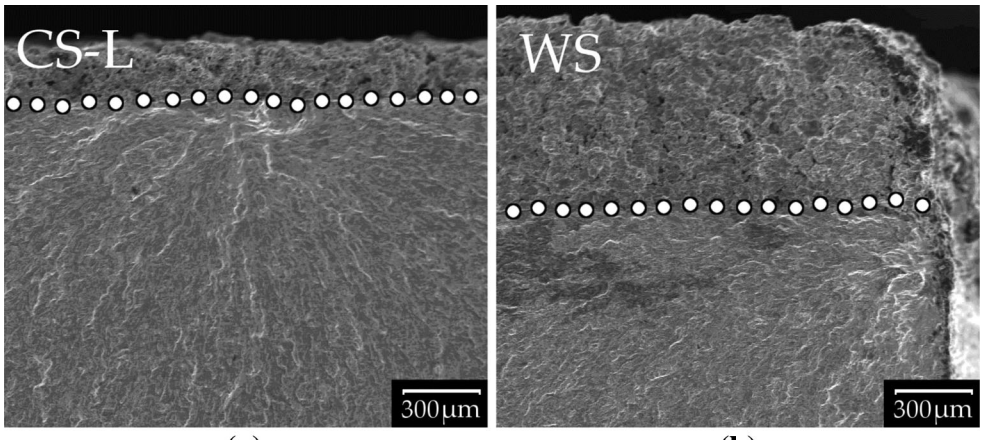

Fig. 9 Illustration of two modes of crack initiation in substrates: (a) perpendicular to major sample face or substrate-coatings interface (typical for AR, GB, PS, and CS sets) and (b) parallel to the substrate-coating interface (typical for WS set). The dots indicate the interface between coatings and substrates

failure of the coating (formation of small particles crushed through contact wear). This was confirmed as no particle fragments were observed in the static rupture regions. Based on the analysis, it can be assumed that the coating fracture surfaces share identical planes with the substrate fatigue cracks and that the fatigue failure of the coatings forms a natural extension of the substrate fatigue cracks. Therefore, the fatigue failures of the coating and substrate are related to each other and propagate concurrently.

The fracture surface of the high-velocity coatings (WS, 2× CS) is interconnected with the respective microstructures. The CS deposits are built up by practically equiaxed particles connected by thin, highly deformed layer of material (as presented by Zou via EBSD observations in (Ref 41)). Their decohesion leads to a formation of fine debris on the fracture surface. Similar failure mechanism can be observed on the whole fracture surface of the WS deposits. However, the amount of particle debris is relatively lower as opposed to both CS coatings. The slight difference is probably connected to the superior compactness of the WS deposit (also observed during the hardness measurements in Fig. 5).

4. Conclusions

The presented study aimed at determination of the effect of deposition of coatings via four thermal spray methods onto fatigue lives of low-carbon steel substrates. It was found that the deposition of coatings by all technologies (plasma, warm, and low-pressure and portable cold sprays) led to a substantial increase in the fatigue lives. The increase in lifetime of the individual sets could be attributed to a presence of fatigue-resistant coatings, introduction of compressive peening stresses, and non-linear behavior of the coating material. Substantial differences in the failure modes of the specimens were observed via fractographic analysis. From the results, it could be concluded that

- Deposition of Ti via portable and low-pressure cold spray technologies did not induce chemical changes into Ti material, as a consequence of the inherent low temperature character of the methods; the extent of particle surface oxidation during the deposition via warm spray is substantially lower as compared to the standard HVOF due to lower temperatures of the process. Plasma deposition led to a complete transformation of Ti into nitrides and oxides.
- Of the three solid-state impact technologies (WS, 2× CS), the Vickers hardness of the cold-sprayed Ti coatings was lower than the values obtained for warm spray deposition. This was caused by fragmentation of the material below the indenter in the cold-sprayed coatings. The highest hardness was measured for PS coatings due to its chemical composition.
- The grit-blasting procedure caused increase in the hardness of the 1.0038 steel substrate material up to depths of ~50 μm. Subsequent deposition of the coatings did not further increase the values.
- Due to easier conformation of the incoming molten Ti particles to surface asperities and the resulting smooth splat surfaces due to the surface tension, the surface roughness of the PS set was lower than the coatings fabricated via the other technologies.
- The grit blasting did not alter the fatigue lives of the specimens due to incidence of two contradictory factors, work hardening of the substrate (compressive stresses) and inherent micro-notches introduction. Therefore, it is suggested that due to the micro-notch effect, grit-blasting procedure should not be carried out prior to cold or warm spray depositions (from the point of view of material fatigue resistance).
- The CTE mismatch of the coatings and the substrates was not the factor causing the increase in fatigue lives of the plasma-sprayed set. Instead, non-linear behavior of the non-compact coatings leading to different stiffness parameters in compression and tension caused effective decrease in the underlying substrate stress amplitude, yielding longer fatigue lives.
- Induction of compressive stresses into the substrates, obliteration of grit blasting-induced micro-notches, and the presence of fatigue-resistant coatings are the main factors causing the increase in fatigue lives of the three high-kinetic energy deposition processes (WS, 2× CS).
- The fatigue crack initiation in substrates favored grit blasting-induced micro-notches. Multiple initiation sites were observed at the major sample faces for AS, GB, 2× CS sets. For the CS coatings, it could not be safely determined whether the primary crack initiated at the substrate-coating interface or the coating surfaces. For PS specimens, single crack propagation from the major face was observed, with the initiation sites close to the specimen edges. In the case of WS deposits, the cracks were constrained to initiate at the specimen edges, completely avoiding the substrate-coating interface areas.

Acknowledgment

The present work has been carried out in NETME Centre, and the authors acknowledge the financial support of European Regional Development Fund under the Operational Programme Research and Development for Innovation. The presented results have been obtained in Netme Centre Plus (LO1202) project co-funded by the Ministry of Education, Youth and Sports in the support programme "National Sustainability Programme I". The support of Czech Science Foundation projects GACR 13-35890S (sample preparation and evaluation) and GACR 108/12/1872 (fatigue testing) is further acknowledged. The main author would like to thank Michal Cizek for providing the schematics of the fatigue test device.

References

1. R. Tucker, Ed., ASM Handbook: Thermal Spray Technology, ASM International, Materials Park, OH, 2013

2. P. Fauchais, Understanding Plasma Spraying, *J. Phys. D*, 2004, **37**(9), p R86-R108
3. J. Cizek, K. Khor, I. Dlouhy, In-flight Temperature and Velocity of Powder Particles of Plasma-Sprayed TiO_2, *J. Therm. Spray Technol.* **22**(8), 2013, p 1320-1327
4. A. Papyrin, V. Kosarev, S. Klinkov, A. Alkimov, and V. Fomin, *Cold Spray Technology*, Elsevier, Oxford, 2007
5. F. Kroupa, Nonlinear Behavior in Compression and Tension of Thermally Sprayed Ceramic Coatings, *J. Therm. Spray Technol.* **16**(1), 2007, p 84-95
6. H. Assadi, F. Gärtner, T. Stoltenhoff, and H. Kreye, Bonding Mechanism in Cold Gas Spraying, *Acta Mater.* **51**(15), 2003, p 4379-4394
7. T. Schmidt, H. Assadi, F. Gärtner, H. Richter, T. Stoltenhoff, H. Kreye, and T. Klassen, From Particle Acceleration to Impact and Bonding in Cold Spraying, *J. Therm. Spray Technol.* **18**(5-6), 794-808 (2009)
8. T. Suhonen, T. Varis, S. Dosta, M. Torrell, and J. Guilemany, Residual Stress Development in Cold Sprayed Al, Cu and Ti Coatings, *Acta Mater.* **61**, 2013, p 6329-6337
9. S. Kuroda, J. Kawakita, M. Watanabe, and H. Katanoda, Warm Spraying—A Novel Coating Process Based on High-Velocity Impact of Solid Particles, *Sci. Technol. Adv. Mater.* **9**, 2008, p 033002
10. R. Ahmed, N. Faisal, S. Knupfer, A. Paradowska, M. Fitzpatrick, K. Khor, and J. Cizek, Neutron Diffraction Residual Strain Measurements in Plasma Sprayed Nanostructured Hydroxyapatite Coatings for Orthopaedic Implants, *Mater .Sci .Forum* **652**, 2010, p 309-314
11. J. Cizek, O. Kovarik, J. Siegl, K. Khor, and I. Dlouhy, Influence of Plasma and Cold Spray Deposited Ti Layers on High-Cycle Fatigue Properties of Ti6Al4V Substrates, *Surf. Coat. Technol.* **217**, 2013, p 23-33
12. R. Musalek, O. Kovarik, T. Skiba, P. Hausild, M. Karlik, and J. Colmenares-Angulo, Fatigue Properties of Fe-Al Intermetallic Coatings Prepared by Plasma Spraying, *Intermetallics* **18**(7), 2010, p 1415-1418
13. R. Souza, M. Nascimento, H. Voorwald, and W. Pigatin, The Effect of WC-17Co Thermal Spray Coating by HVOF and Hard Chromium Electroplating on the Fatigue Life and Abrasive Wear Resistance of AISI 4340 High Strength Steel, *Corros. Rev.* **21**(1), 2003, p 75-96
14. K. Binder, J. Gottschalk, M. Kollenda, F. Gärtner, and T. Klassen, Influence of Impact Angle and Gas Temperature on Mechanical Properties of Titanium Cold Spray Deposits, *J. Therm. Spray Technol.* **20**(1-2), 2011, p 234-242
15. T. Price, P. Shipway, and D. McCartney, Effect of Cold Spray Deposition of a Titanium Coating on Fatigue Behavior of a Titanium Alloy, *J. Therm. Spray Technol.* **15**(4), 2006, p 507-512
16. R. Ghelichi, D. MacDonald, S. Bagherifard, H. Jahed, M. Guagliano, and B. Jodoin, Microstructure and Fatigue Behavior of Cold Spray Coated Al5052, *Acta Mater.* **60**(19), 2012, p 6555-6561
17. D. Helfritsch and M. Trexler, How Operating Parameters and Powder Characteristics Affect Cold Spray Costs, *North American Cold Spray Conference*, 2011
18. H. Fukanuma, N. Ohno, B. Sun, and R. Huang, In-flight Particle Velocity Measurements with DPV-2000 in Cold Spray, *Surf. Coat. Technol.* **201**(5), 2006, p 1935-1941
19. O. Kovarik, P. Hausild, J. Siegl, Z. Pala, J. Matejicek, and V. Davydov, The Influence of Plasma Sprayed Multilayers of Cr_2O_3 and Ni10wt.%Al on Fatigue Resistance, *Surf. Coat. Technol.* **251**, 2014, p 143-150
20. E. Degarmo, J. Black, and R. Kohser, *Materials and Processes in Manufacturing*, 9th ed., Wiley, New York, 2003
21. J. Wigren, Grit Blasting as Surface Preparation Before Plasma Spraying, *Surf. Coat. Technol.* **34**(1), 1988, p 101-108
22. C. Leinenbach and D. Eifler, Fatigue and Cyclic Deformation Behaviour of Surface-Modified Titanium Alloys in Simulated Physiological Media, *Biomaterials* **27**(8), 2006, p 1200-1208
23. D. Brunette, P. Tengvall, M. Textor, and P. Thomsen, *Titanium in Medicine*, Springer, Berlin, 2001
24. International Organization for Standardization, ISO Standard 4287: Geometrical Product Specifications—Surface Texture: Profile Method—Terms, Definitions and Surface Texture Parameters, 1997
25. D. Chicot, H. Ageorges, M. Voda, G. Louis, M.B. Dhia, C. Palacio, and S. Kossman, Hardness of Thermal Sprayed Coatings: Relevance of the Scale of Measurement, *Surf. Coat. Technol.*, 2014
26. H. Rietveld, Line Profiles of Neutron Powder-Diffraction Peaks for Structure Refinement, *Acta Cryst.* **22**, 1967, p 151-152
27. O. Kovarik, J. Siegl, and Z. Prochazka, Fatigue Behavior of Bodies with Thermally Sprayed Metallic and Ceramic Deposits, *J. Therm. Spray Technol.* **17**(4), 2008, p 525-532
28. M. Meggiolaro and J. Castro, Statistical Evaluation of Strain-Life Fatigue Crack Initiation Predictions, *Int. J. Fatigue* **26**, 2004, p 463-476
29. P. Fauchais, M. Fukumoto, A. Vardelle, and M. Vardelle, Knowledge Concerning Splay Formation: An Invited Review, *J. Therm. Spray Technol.* **13**(3), 2004, p 337-360
30. O. Kovarik, J. Siegl, J. Nohava, and P. Chraska, Young's Modulus and Fatigue Behavior of Plasma-Sprayed Alumina Coatings, *J. Therm. Spray Technol.* **14**(2), 2005, p 231-238
31. D. Goldbaum, J. Ajaja, R. Chromik, W. Wong, S. Yue, E. Irissou, and J. Legoux, Mechanical Behavior of Ti Cold Spray Coatings Determined by a Multi-scale Indentation Method, *Mater. Sci. Eng. A* **530**, 2011, p 253-265
32. M. Mellali, A. Grimaud, A. Leger, P. Fauchais, and J. Lu, Alumina Grit Blasting Parameters for Surface Preparation in the Plasma Spraying Operation, *J. Therm. Spray Technol.* **6**(2), 1997, p 217-227
33. K. Chander, M. Vashista, K. Sabiruddin, S. Paul, and P. Bandyopadhyay, Effects of Grit Blasting on Surface Properties of Steel Substrates, *Mater. Des.* **30**(8), 2009, p 2895-2902
34. G. Lutjering and J. Williams, *Titanium*, 2nd ed., Springer, Berlin, 2007
35. L. Zhu, J. He, D. Yan, L. Xiao, Y. Dong, J. Zhang, and H. Liao, Synthesis and Microstructure Observation of Titanium Carbonitride Nanostructured Coatings Using Reactive Plasma Spraying in Atmosphere, *Appl. Surf. Sci.* **257**(20), 2011, p 8722-8727
36. L. Xiao, D. Yan, J. He, L. Zhu, Y. Dong, J. Zhang, and X. Li, Nanostructured TiN Coating Prepared by Reactive Plasma Spraying in Atmosphere, *Appl. Surf. Sci.* **253**(18), 2007, p 7535-7539
37. A. Kobayashi, Formation of TiN Coatings by Gas Tunnel Type Plasma Reactive Spraying, *Surf. Coat. Technol.* **132**(2-3), 2000, p 152-157
38. M. de Strycker, L. Schueremans, W. van Paepegem, and D. Debruyne, Measuring the Thermal Expansion Coefficient of Tubular Steel Specimens with Digital Image Correlation Techniques, *Opt. Lasers Eng.* **48**, 2010, p 978-986
39. D. Hummer, P. Heaney, and J. Post, Thermal Expansion of Anatase and Rutile Between 300 and 575 K Using Synchrotron Powder x-ray Diffraction, *Powder Differ.* **22**, 2007, p 352-357
40. R. Musalek, J. Matejicek, M. Vilemova, and O. Kovarik, Nonlinear Mechanical Behavior of Plasma Sprayed Alumina Under Mechanical and Thermal Loading, *J. Therm. Spray Technol.* **19**(1-2), 2010, p 422-428
41. Y. Zou, ''Microstructural studies of cold sprayed pure nickel, copper and aluminum coatings,'' Master's thesis, McGill University, 2010